Employing Radical Motion in a Quantum Avian Compass Model to Enhance Sensitivity

Nahnsu Dawkins

Supervisor: Daniel Katnig

Project Partner: Iona Peasgood

18th May 2020

Abstract

Though the phenomenon of avian magnetoreception during migration has been long established, the exact mechanism behind it has not been fully explained. The radical pair mechanism (RPM) is a credible and well-supported theory that describes how a weak magnetic field could be detected with organic materials through quantum effects. However, mutually exclusive conditions for high sensitivity have prevented RPM models from being able to replicate the sensitivity measured in vivo. By adding radical motion to an RPM toy model these self-limiting effects were mitigated. Both oscillatory motion and Brownian motion were tested and found to improve sensitivity. Optimization techniques reveal intense motion within the first 6 μs of the simulation to have the largest impact on sensitivity.

Contents

1 Introduction

1.1 Avian Migration

Avian migration is a peculiar phenomenon in which birds travel many thousands of miles in order to mate, find food, or avoid harsh weather. Along some of these migration routes birds display an ability to travel, during both day and night, across large areas of featureless ocean or desert, correcting course when displaced [1]. This indicates that they are not only using visual and olfactory markers to form a map, but also have an internal compass by which they are able to determine their orientation, thus allowing them to perform true navigation [2]. Experiment reveals that birds are sensitive to magnetic fields on the order of the Earth's magnetic field (50 μT) [3], supporting the hypothesis that they are detecting and using this field during migration. Their method of detection also seems to require light, as their use of a magnetic compass in course correction is inhibited at night [4].

The Earth's magnetic field does not usually have an impact on biological systems because it is so weak: the effect of thermal fluctuations is far stronger than any interactions between organic matter and the field [5]. This raises the question of how birds could be using this field to navigate, as they do not contain high levels of ferromagnetic materials that would facilitate this, nor a particular organ that might help in this domain.

1.2 The Radical Pair Mechanism

While a weak field is unlikely to have an effect on its own, it might bias the final state of a system far from equilibrium, where there are several equally possible outcomes. Consider the analogy of a heavy block and a fly, as in Fig. 1. If the block is stable, a fly landing on the rock would have little to no effect on its position. However, if the rock is far from an equilibrium, for example balanced on a point from which it will fall on either of its sides, then the fly could be the deciding factor in the block's final orientation.

Schulten *et al.* first proposed an analogous chemical mechanism for avian magnetoreception in 1978, in which a chemical reaction with a magnetically sensitive transient radical pair had a final yield dependent on the direction of an external magnetic field [6] (shown in Fig. 2). Biologists were initially skeptical of this idea, since there were no clear candidates for chemicals that would undergo this process and little precedent for quantum mechanical effects to have impact on biological systems.

Research into the radical pair mechanism was reinvigorated when a suitable material was found, thus giving credibility to the theory and allowing precise models of the mechanism to be de-

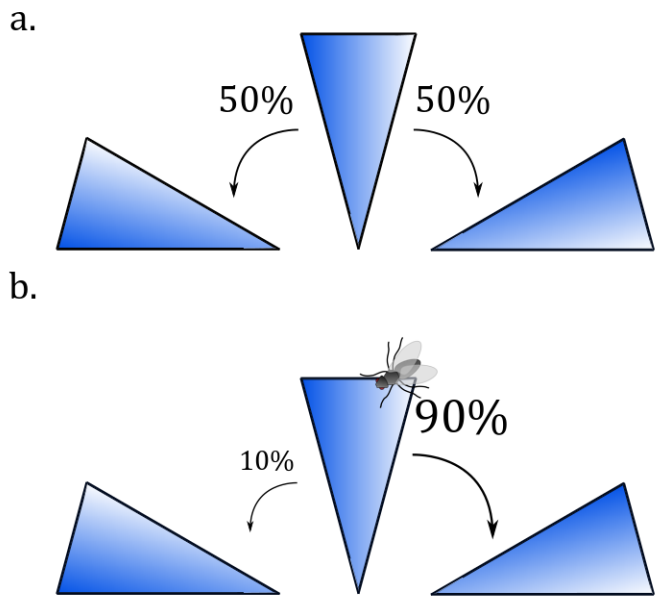

Figure 1: An analogy for the radical pair mechanism, by which a light fly can impact a heavy block if it is in an unstable state.
a) A block in a state far from equilibrium, which has equal chance of falling into one of two equilibrium states.
b) A fly affecting a heavy block much more than their comparative weights would otherwise indicate, due to the block's instability.

veloped. Cryptochrome, a light sensitive protein found in the bird's eye, was found to form a radical pair when exposed to blue light [7]. The radicals produced are a flavin adenine dinucleotide, $FAD^{\cdot -}$, and a triad of tryptophan amino acids, $Trp^{\cdot +}$ (Fig. 3). The radical pair is created when blue light breaks a chemical bond, exciting the FAD and Trp. This causes electron transfer from the triad to the FAD, such that one free electron is at each site, to form the radical pair.

The radicals, previously required to have complementary spins, can now have anti-parallel (singlet) or parallel (triplet) spin. These spin states are so named because there is one singlet state: $S_0 = \frac{1}{\sqrt{(2)}}((\uparrow_1\downarrow_2) - (\downarrow_1\uparrow_2))$ and three triplet states: $T_{+1} = (\uparrow_1\uparrow_2)$, $T_0 = \frac{1}{\sqrt{2}}((\uparrow_1\downarrow_2) + (\downarrow_1\uparrow_2))$, $T_{-1} = (\downarrow_1\downarrow_2)$. Conversion between these states is more likely when their energies are comparable.

Radicals are unstable and soon will combine with other materials, either collapsing back to their original components or going on to form a new compound (shown in Fig.2). The radicals are created in the singlet state and can only form their original bond from this state, due to spin conservation. However, with hyperfine interactions between the radicals and nearby nuclear spin, the radicals undergo singlet-triplet (S-T) interconversion, oscillating between the two states [6].

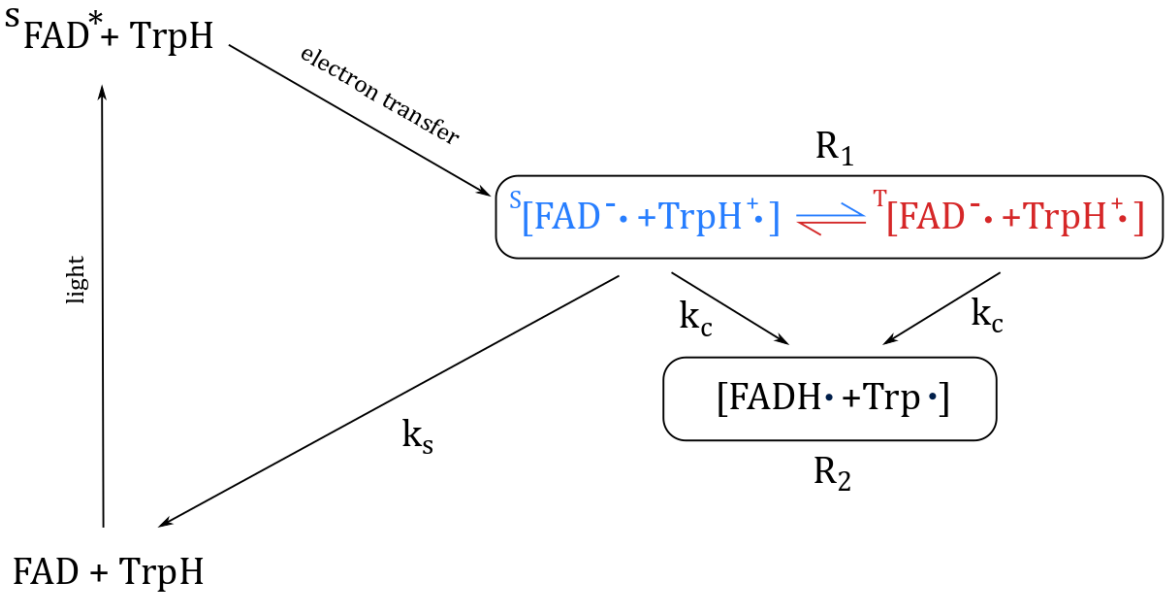

Figure 2: The process by which a radical pair is created and yields different chemical products depending on an external magnetic field. k_s is a spin-selective back reaction and k_c a non-spin selective forward reaction, both on the order of μs. The more radicals in the triplet state there are due to S-T interconversion, the more radicals are forced into the forward reaction, excluded by the spin-selectivity of k_s. Importantly, though R_2 is another radical pair, it does not experience magnetic field effects as R_1 does.

This nuclear spin could be supplied by nitrogen or hydrogen, which are common in biological matter and exist in cryptochrome [8]. When in the triplet state, exchange interactions forbid the radicals from recombining with each other, and so they form novel compounds. The yields of the final compounds produced could be the basis of a bio-signal in the bird, perhaps acting as a filter over its normal vision (as cryptochrome is located in the ultraviolet cones of many birds [9]). Because this process is driven by the spins of the radicals, which are not thermally equilibrated, the small relative strength of the field is no longer so prohibitive to its detection by organic materials. In order for this mechanism to work the rates of recombination (k_c and k_s) need to be approximately equal, as otherwise most of the radicals will form the products of the dominant reaction.

The radicals are also sensitive to an externally applied magnetic field through the Zeeman effect, which causes singlet-triplet interconversion to be further modified when exposed to such fields. Since the molecules involved are anisotropic, the direction of the magnetic field also factors into the amount and type of modulation, as shown in Fig.4. The change in the rate of interconversion affects the triplet population, which in turn affects the final yield of different chemicals that go

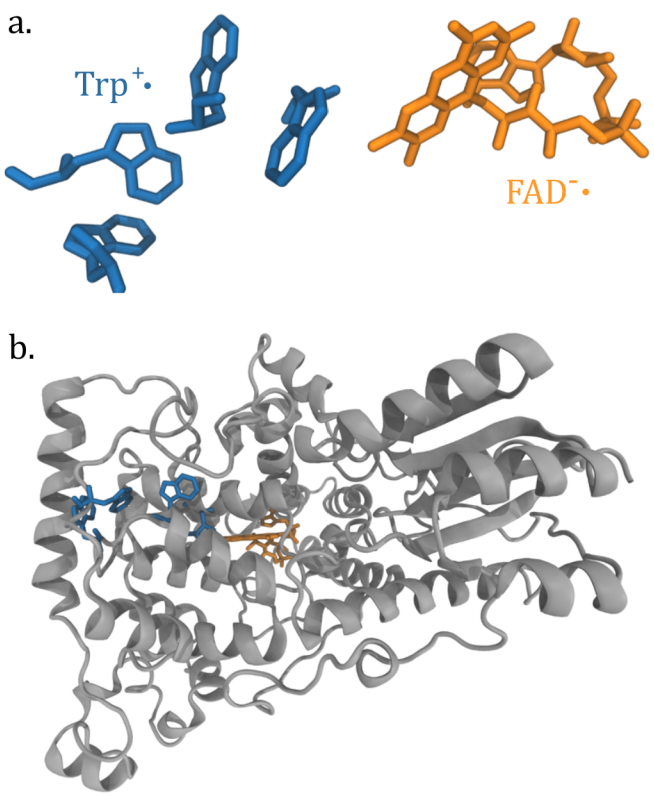

Figure 3: a) Visualization of the three Trp and FAD molecules that form the radicals in a cryptochrome RPM.
b) Positioning of the radicals in the cryptochrome protein.

on to produce biological signals. The difference in final yields at different field orientations is what would allow birds to navigate using the Earth's magnetic field. The more anisotropic this result is, the more sensitive this mechanism to the direction of the Earth's magnetic field.

Another phenomenon that further supports RPM is the disruption of avian magnetoreception in the presence of a very weak resonant magnetic field [10]. When birds were exposed to a magnetic field oscillating at the Larmor frequency (1.4 MHz on average in the Earth's magnetic field), their ability to detect the Earth's field was disrupted, with a resonant field strength of 15 nT being enough to achieve this effect [11]. Other chemical reactions dependent on a transient radical pair have been shown to be similarly sensitive to very weak resonance magnetic field [12]. This phenomenon is known as reaction yield detected magnetic resonance, or RYDMR, and is not predicted for other models of avian magnetoreception. It requires a field oscillating at the same frequency as the S-T interconversion show in Fig. 4. This extreme sensitivity of the RPM model to resonant fields could explain the disruptive influence of man-made electromagnetic noise (or electrosmog) on migratory birds at close range [13].

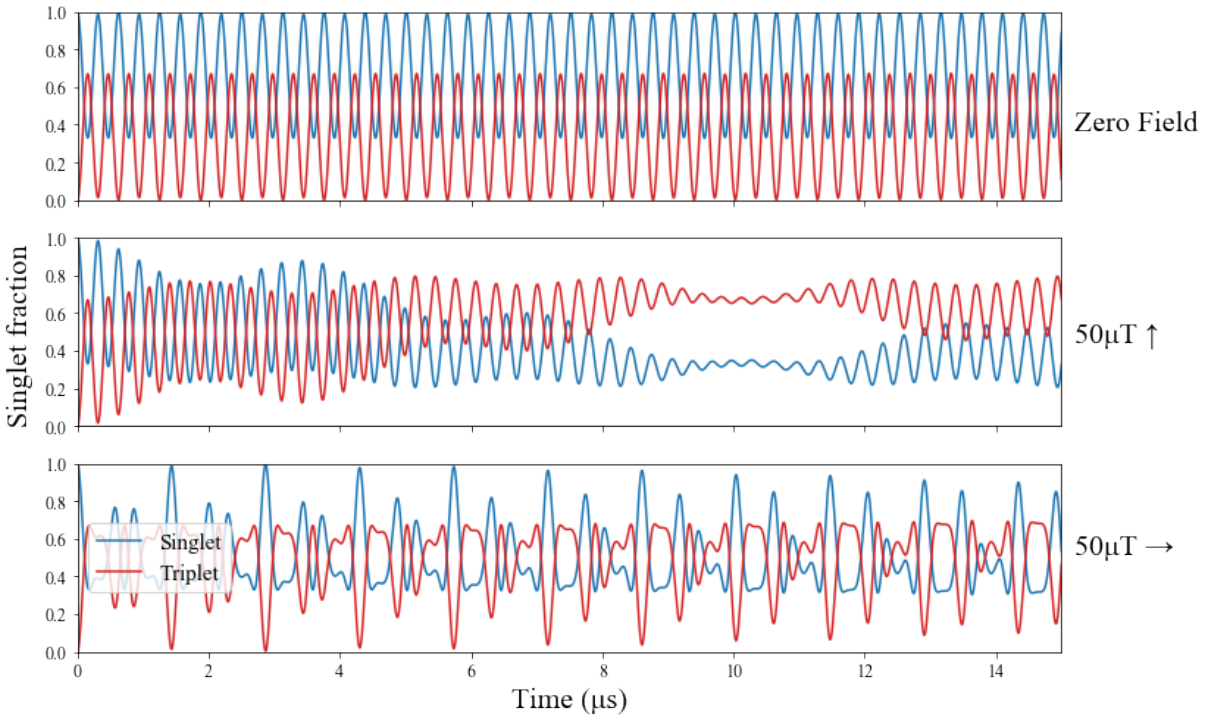

Figure 4: The oscillating singlet and triplet spin populations with no external magnetic field, a z-axis field, and an x-axis field. This simulation excluded recombination or exchange interactions and has an external field strength of 50 μT.

1.3 Radical Motion in RPM

While the RPM describes many aspects of the avian compass, its predicted sensitivity is below what would be required for detection of the Earth's magnetic field in many contexts. This is primarily because of the mutually exclusive requirements for high sensitivity: slow recombination and strong exchange interactions [14]. Without slow recombination, singlet-triplet interconversions have limited time to take place, and the majority of the population remains in the singlet state, vastly reducing sensitivity. Slow recombination can be achieved with a larger distance between radicals. However, a larger distance between radicals lowers the strength of exchange interactions, which instigate S-T interconversion and are vital to the functioning of this mechanism. A solution could be radical motion, in an attempt to fulfill both of these requirements for high sensitivity. The exploration of the impact of time-dependent radical distance variation on a RPM toy model is the primary goal of this project.

1.4 Mathematical Model

1.4.1 Two Radicals and a Nuclear Spin

In this project we iterated through models of increasing complexity as more components of the system were included in simulations. Initially, we considered a system of two radicals,

influenced by a nuclear spin through hyperfine interactions and by an external magnetic field through Zeeman interactions, without recombination, which has spin Hamiltonian

$$\hat{H}_0 = \hat{H}_{\text{Zeeman}} + \hat{H}_{\text{hyperfine}} = \boldsymbol{\omega}(\hat{S}_{Az} + \hat{S}_{Bz}) + \boldsymbol{A} \cdot \hat{I} \cdot \hat{S}_A \tag{1}$$

where $\boldsymbol{\omega}$ is the Larmor frequency, S_A and S_A each being the spin operator of a radical, $\hat{I}$ being the nuclear spin, and $\boldsymbol{A}$ the anisotropy of the molecule. The Lamor frequency can be found with $\boldsymbol{\omega} = \gamma \boldsymbol{B_0}$, where γ is the gyromagnetic ratio of the radicals and $\boldsymbol{B_0}$ is the applied magnetic field [15].

The probability of being in the singlet state is

$$p_S(t) = Tr[\hat{\boldsymbol{\rho}}(t)\hat{P}_S(t)] \tag{2}$$

where $\hat{\boldsymbol{\rho}}(t)$ is the spin density operator, and $\hat{P}_S$ is the singlet state projection operator. The probability of being in the singlet and triplet states are complementary, such that

$$p_T(t) = 1 - p_S(t) \tag{3}$$

We can find the state projection operator with

$$\hat{P}_S = \frac{1}{4}I - \hat{S}_A \cdot \hat{S}_B \tag{4}$$

and find $\hat{\boldsymbol{\rho}}(t)$ with the Liouville-von Neumann equation

$$\dot{\boldsymbol{\rho}} = -i[\hat{H}, \boldsymbol{\rho}] \tag{5}$$

1.4.2 Recombination and Exchange Interactions

When recombination is introduced to the model, the relevant Liouville-von Neumann equation is modified such that

$$\dot{\boldsymbol{\rho}} = -i[\hat{H}, \boldsymbol{\rho}] - K\boldsymbol{\rho} \tag{6}$$

where $K = \frac{k_s}{2}\hat{P}_S + \frac{k_c}{2}\hat{P}_T$, with k_S and k_C as previously defined in Fig.2. Considering that they are approximately equal, this can be rearranged to

$$\dot{\boldsymbol{\rho}} = -i[(\hat{H} - i\frac{k_s}{2}\hat{P}_S), \boldsymbol{\rho}] \tag{7}$$

and it becomes clear that we can implement this by using an effective Hamiltonian

$$\hat{H}_{\text{eff}} = \hat{H} - i\frac{k_s}{2}\hat{P}_s \tag{8}$$

The yield over the course of our simulation can be found by integrating the probability and recombination rate over time, as such,

$$\Phi_s = \int_0^{t_f} k_s p_s dt \tag{9}$$

Timmel *et al.* in their 2011 paper [15] find that, analytically, such a model produces a singlet yield

$$\begin{aligned}\Phi_S = &\frac{3}{8} + \frac{1}{8}\frac{\omega^2}{\Omega^2}\left[1 + f(\omega)\right] \\ &+ \frac{1}{8}\left(1 - \frac{\omega}{\Omega}\right)\left[f\left(\tfrac{1}{2}a + \tfrac{1}{2}\omega + \tfrac{1}{2}\Omega\right) + f\left(\tfrac{1}{2}a - \tfrac{1}{2}\omega - \tfrac{1}{2}\Omega\right)\right] \\ &+ \frac{1}{8}\left(1 + \frac{\omega}{\Omega}\right)\left[f\left(\tfrac{1}{2}a - \tfrac{1}{2}\omega + \tfrac{1}{2}\Omega\right) + f\left(\tfrac{1}{2}a + \tfrac{1}{2}\omega - \tfrac{1}{2}\Omega\right)\right]\end{aligned} \tag{10}$$

where ω is the Larmor frequency, $\Omega = \sqrt{a^2 + \omega^2}$, and $f(x) = \frac{k^2}{k^2+x^2}$. These are results we shall try to reproduce computationally before modelling more aspects of the system.
Next, the exchange interactions between the radicals is added, which will have the Hamiltonian

$$\hat{H}_{\text{ex}} = -J\left(\frac{1}{2} + 2\hat{S}_A\hat{S}_B\right) \tag{11}$$

where J is the exchange interaction strength. This will further modify our effective Hamiltonian.

This project models the hyperfine and Zeeman interactions, the recombination of the radicals, and exchange terms between radicals. The dipole-dipole interactions between radicals will not be modelled, as this adds significant complexity and computation time, surpassing the resources and scope of this project. However, the results of a RPM with radical motion model with dipole interactions will be briefly discussed, with data obtained from Daniel Kattnig.

1.4.3 Radical Motion

Radical motion will change two aspects of the model, the exchange interaction and the recombination rate. Each is affected by the addition of a time-dependent radical distance such that

$$K \longrightarrow k_{s0}e^{-\beta r(t)} \tag{12}$$

$$J \longrightarrow J_0 e^{-\beta r(t)} \tag{13}$$

where k_S and J_0 are the values of K and J at time zero, and β is a parameter determining how strongly the radical distance affects them [16].

The oscillatory style motion will follow the equation

$$r(t) = \frac{A}{2}(1 - \cos(ft)) \tag{14}$$

where A is the amplitude and f is the frequency. The random motion will follow the Langevin equation for a particle in a fluid medium

$$m\frac{dv}{dt} = \xi v + \delta F(t) \tag{15}$$

where m is the mass, v is the velocity, ξ is a frictional coefficient for the particle and its medium, and $\delta F(t)$ is a small, functionally random force felt by the particle [17].

2 Methods

2.1 Building and Validating Model

Before experimenting with a computational RPM model, it was first necessary to validate it against other models, as previously discussed. The model was developed iteratively, first with hyperfine and Zeeman interactions, then with recombination, and finally with exchange interactions. Following that, the novel aspect of the model was added, a time dependent radical distance that varied the recombination rates and strength of exchange interactions.

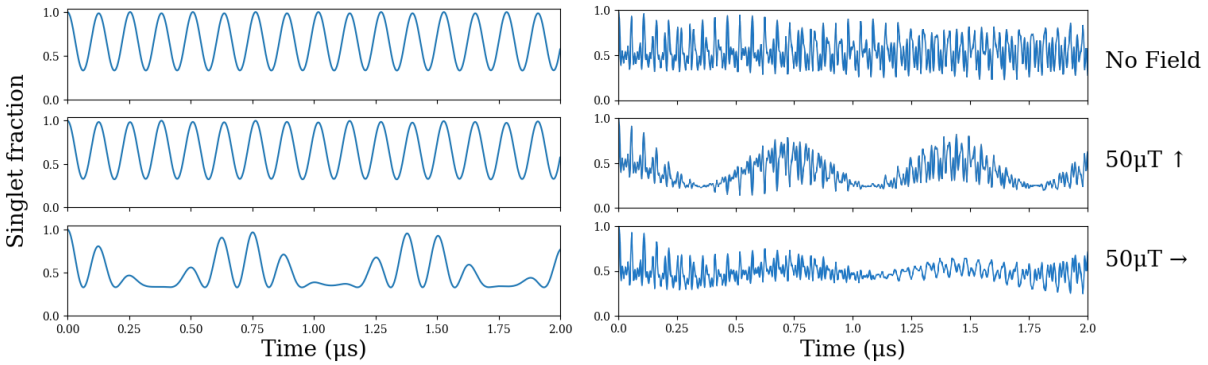

(a) Data produced in this project

(b) Data from [5]

Figure 5: A comparison of data from Hore's and Mouritsen's paper [5] with data produced with the computational model of this paper, plotting the fraction of radicals in the singlet state against time. Both models include hyperfine and Zeeman interactions, but do not include exchange interactions or radical recombination. The effect of no field, a z-axis field, and an x-axis field upon the singlet population is shown.

A model without recombination or exchange interactions was compared to data from P.J. Hore and Henrik Mouritsen's 2016 paper [5]. As seen in Fig. 5, our model replicates the oscillating populations of S-T interconversion and the regular modulation caused by a magnetic field. In both graphs one can see the difference in interconversion caused by the direction of the magnetic

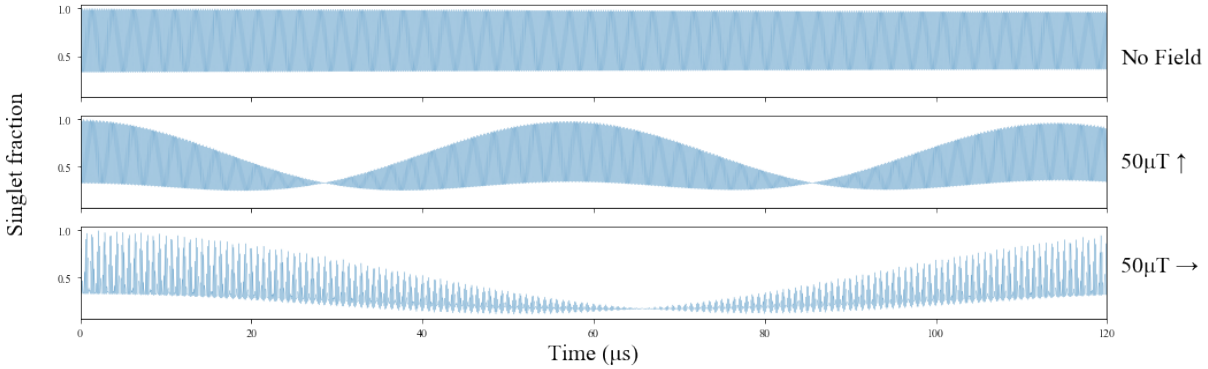

Figure 6: Data from this project similar to Fig. 5, but over a longer timescale to show similatires to Hore's data.

field, with the modulation of a z-axis field being very regular and an x-axis field being more complex. However, our results differ in the frequency of oscillation and modulation, with these frequencies being much higher in Hore's graphs. While the overall trends remain the same, the patterns seen in Hore's graphs (Fig. 5b) occur over a much longer timespan in our data (Fig. 6).

When recombination is added to simulations the final yield can be calculated, and again we compare our data to Hore's and Mouritsen's (Fig. 7). Here, our model replicate their data more closely, with the most important aspect, the yield anisotropy, being comparable in magnitude (though slightly larger in our case).

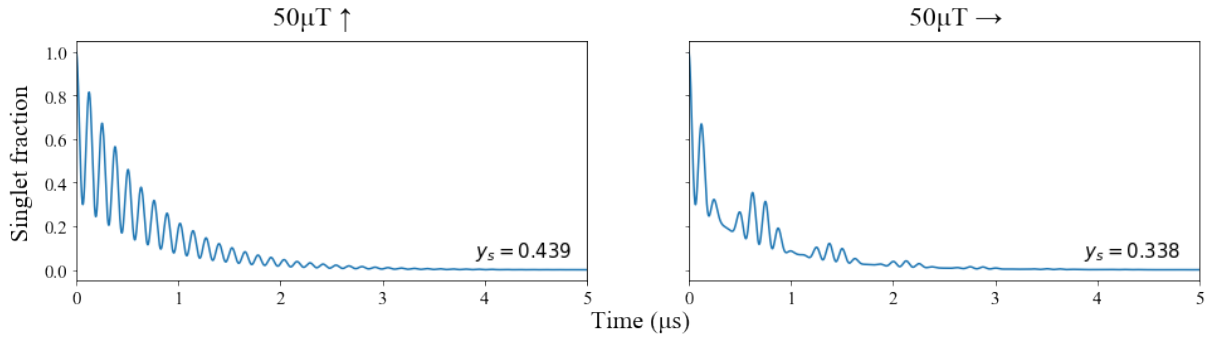

(a) Data produced in this project

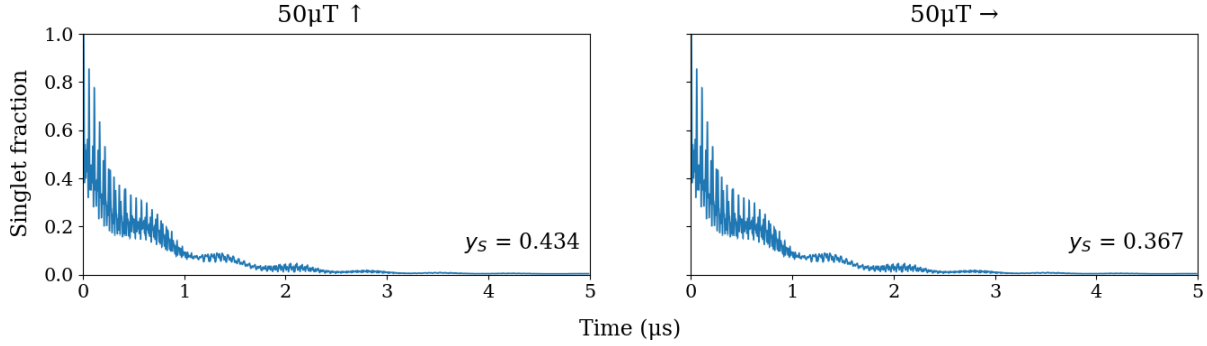

(b) Data from [5]

Figure 7: A comparison of data from Hore's and Mouritsen's paper [5] with data produced with the computational model of this paper, including recombination. y_s is the singlet yield.

This recombination inclusive model should also output yields comparable to those predicted in Timmel's 2011 paper [15] as laid out in equation 10, which it replicates well within computational error (Fig. 8). Though some features of our singlet-triplet interconversion model seem to differ from those of Hore's, the replication of Timmel's analytical value for singlet yield indicates the validity of the model.

The addition of time dependent exchange interactions and recombination is achieved through creating a set of Liouvillian functions, which we then solve for (rather than our Hamiltonian), with $L(L_{\text{eff}}, K(r(t)), L_{\text{ex}}(J(r(t)))$, with K and J as in equations 12 and 13. The variation in radical

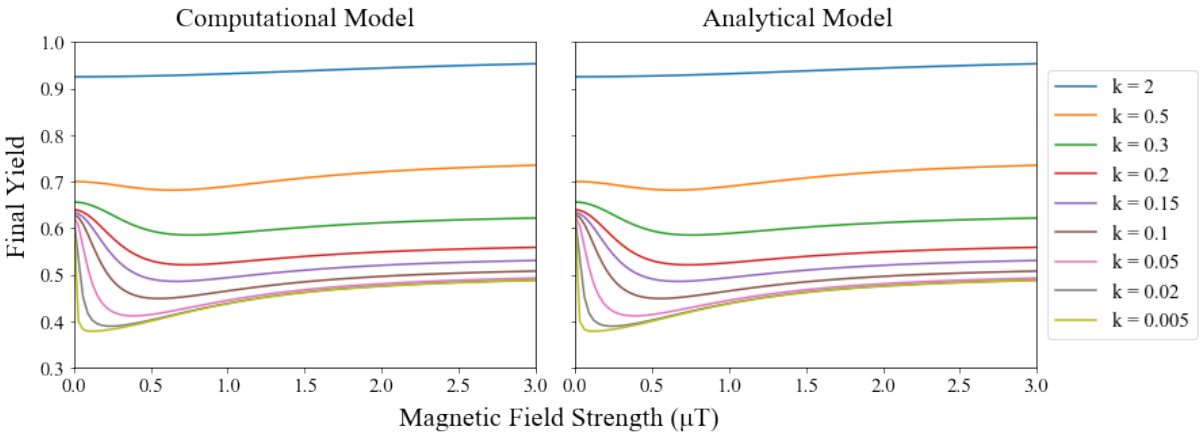

Figure 8: A comparison of data from Timmel's paper [15] with data produced with the computational model of this paper. These compute the final yield for a variety of recombination rates (k), varying from 0.005 to 2. Differences between the computational and analytical models are well within computational resolution.

distance will be on the order of ångströms, as it is feasible that radicals in the cryptochrome would be able to travel the distance of several atoms [18]. The types of motion tested will be oscillatory motion and Brownian motion, the latter of which will be simulated by the Langevin equation (and primarily done by my project partner). Much of my own work focused on finding the optimum radical motion and its properties.

2.2 Optimization Methods

With a working and validated model, various parameters can now be optimized in order to try and find the radical motion that produces the highest yield anisotropy. There are several parameters against which we can try and optimize sensitivity. Assuming oscillatory motion, the amplitude and frequency are these parameters. However, by treating the distance at each timestep as a parameter, no motion type need be assumed, allowing the radicals to be anywhere (within a reasonable range) over the simulated time. Though this might output a nonphysical result, it will hopefully reveal what type of motion is conductive to high RPM sensitivity. Minimization functionality from the scipy.optimize Python module will be used, minimizing the negative of the yield anisotropy, with a penalty imposed for straying outside of reasonable distances.

Python has various minimization methods available for use. For optimization of the oscillatory motion model the Nelder-Mead, Powell, conjugate gradient, BFGS, and limited memory BFGS (LM-BFGS) algorithms were tested. The Powell algorithm was used for assumed oscillatory motion, as it outperformed all but LM-BFGS by ~232%, and outperformed LM-BFGS by ~19%. However, because the problem of optimizing the distance over each timestep has

high non-linearity and many parameters, we could not use many of the faster methods (such as Powell or CG). Instead the slower but more robust Nelder-Mead method was used. Since the minimization function requires initial values for its parameters, a variety were tested as an attempt to screen out potential undesirable local minima. The parameters were the distances at each timestep, with initial values generated from quantization of some function of time. The initial 'guess' functions used here were the oscillatory motion mentioned above, an exponential approach, and that of stationary radicals (as shown in Fig. 12 and 14).

In solving for the distance at each timestep, the task needs to be separated into two functions: an output function that returns the yield and a minimizing function that minimizes the yield against the parameters. This division is required because the output function will need arguments other than the parameters (such as initial guess values, acceptable error, etc.), and the minimize functionality requires that the only argument be the parameters.

In the output function, we first define the penalty ascribed to radicals that stray too far from each other. Here, we used

$$\text{penalty} = \frac{1}{2}\left(1 + \tanh\left(\frac{r_{max} - r}{p}\right)\right) \cdot \frac{1}{2}\left(1 + \tanh\left(\frac{r - r_{min}}{p}\right)\right) \tag{16}$$

where r_{max} and r_{min} are the maximum and minimum of our initial guess radical distance functions, r is the radical distance, and p is a parameter determining how harsh the penalty is for straying outside of the limits, with a low p corresponding to a harsh penalty. The function then evaluates the singlet yield under a magnetic field along the z-axis and x-axis, and returns the negative difference (multiplied by the penalty).

In the minimizing function we state our initial guess value for the parameters and find r_{max} and r_{min}. Most importantly, a function that calls the output function with only the parameters as arguments is defined, and this function is then minimized with respect to its arguments.

When we attempted to find the optimized radical motion with no assumed motion type, there were many parameters to optimize against. This severely inhibited the performance of our minimization algorithm and increased the computation time such that data collection became unfeasible in the scope of time for this project. Thus, a thinning factor, F was introduced, such that instead of finding the radical distance at every timestep, the radical distance at every T/F timesteps was found, where T is the number of timesteps. This creates a lower resolution, more expedient result.

3 Results and Discussion

3.1 Oscillatory Radical Motion

Two different types of oscillatory radical motion improved the yield anisotropy: a slow and high amplitude oscillation and a quick and small amplitude oscillation. This improvement is demonstrated in Fig. 9, which shows the effect of oscillatory motion by varying oscillation frequency and amplitude. A stationary radical is modelled by a zero amplitude oscillation. The anisotropy of this model seems to peak at certain frequencies for all non-zero amplitudes. This perhaps indicates resonances of the system, similar to the phenomenon in RYDMR.

	Peak 1	Peak 2	Peak 3	Peak 4	Peak5	Peak 6
Average Frequency (MHz)	0.568	1.21	3.25	4.71	6.29	9.25
Frequency Variance (kHz)	9.18	5.10	0.256	0.0640	0.104	6.02
Average Anisotropy (10^{-2})	9.24	6.23	5.78	6.28	5.48	4.96
Anisotropy Variance (10^{-5})	1.09	4.96	1.61	8.91	7.88	7.33

Amplitude (Å)	0	2	4	6	8	10
Anisotropy (Average)	0.0491	0.0643	0.0534	0.0465	0.0419	0.0385

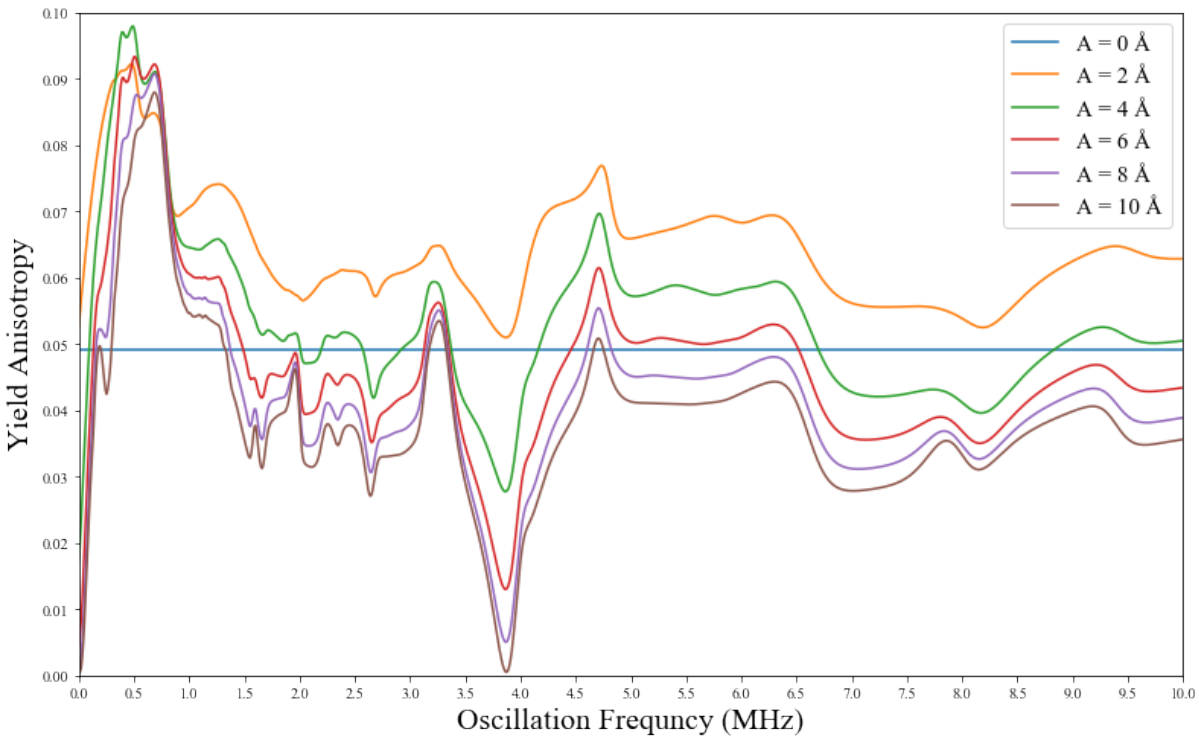

Figure 9: The effect of the frequency and amplitude of oscillation of radical motion, A, on the RPM model.

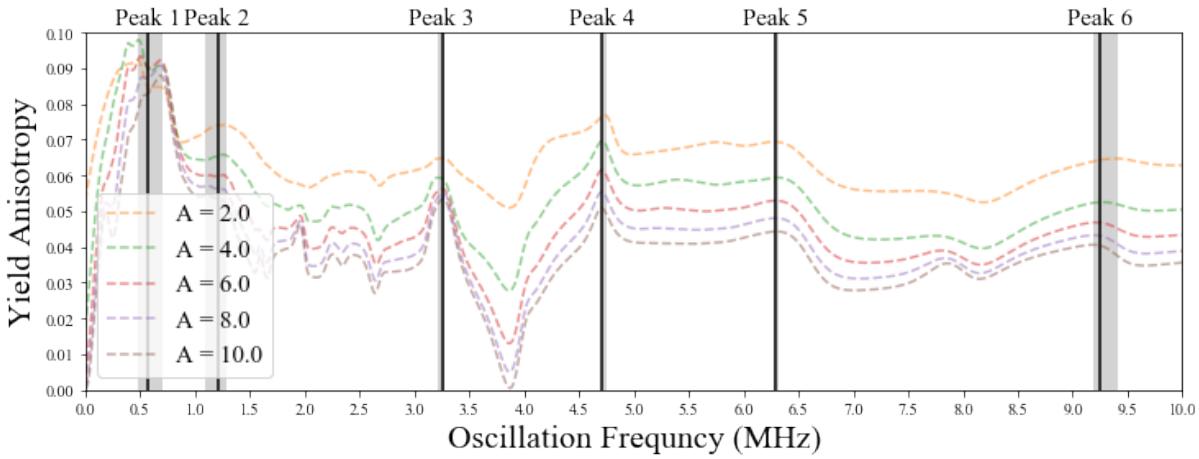

(a) The peaks in yield anisotropy at certain frequencies found in an RPM model with radical motion. Grey areas indicate minimum to maximum position of the peak from different non-zero amplitudes.

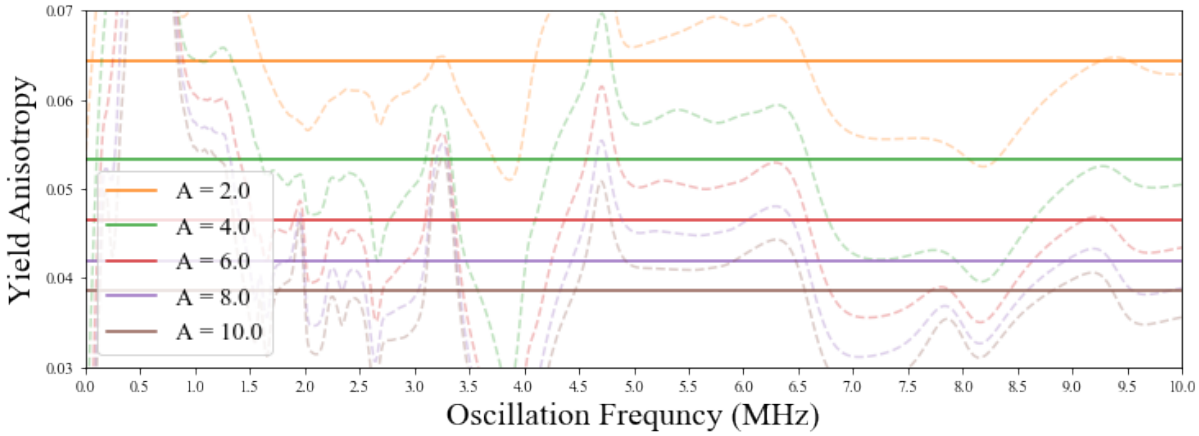

(b) The average yield anisotropy for different amplitudes oscillations. Values seem to converge as amplitude increases.

Figure 10: Replication of Fig. 9, with focus on
a) the position of the peaks and their variance and
b) the mean yield anisotropy of each amplitude

From the data above, we see that the lowest non-zero amplitude (2 Å) has the highest average anisotropy and that the anisotropy falls as the amplitude increases. Above 6 Å, on average, the improvement from radical motion is removed. The only place where large amplitudes seem advantageous is near Peak 1, at ~0.57 MHz (peaks shown in Fig.10a). A closer look at this area of interest is plotted in Fig. 11, which reveals that in this area higher amplitudes do indeed have higher yield anisotropy. Additionally, one can see that this first peak seems to diverge at lower amplitude oscillations into two sub-peaks, one at ~0.48 MHz and one at ~0.69 MHz.

The fact that peaks are common to all amplitudes and have low variance suggest that they indicate resonant frequencies of the radical pair. However, these frequencies do not have a clear relationship to the Larmor frequencies, unlike the phenomenon of RYDMR, in which there is a

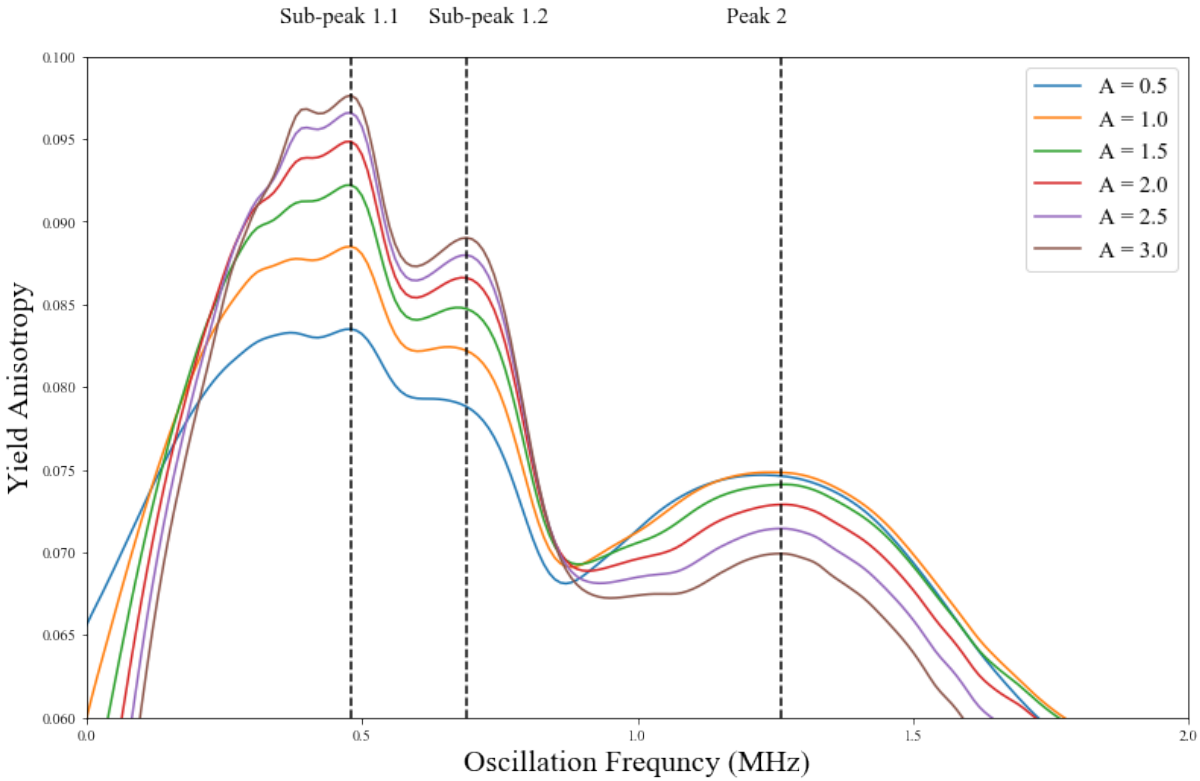

Figure 11: A closer look at peaks 1 and 2 as indicated on Fig. 9, in order to demonstrate the inversion of usual trends at peak 1, where a larger amplitudes results in larger anisotropy. The presence of two distinct peaks that form Peak 1 also becomes clearer.

significant peak at the Larmor frequency (1.4 MHz). Peaks also seem to be getting farther and farther away from each other (though few data points make this hard to distinguish), which is not a phenomenon found in RYDMR.

At the highest peak the yield anisotropy is approximately doubled due to radical motion. However, on an absolute scale, this is only an increase of around 0.05. Whether or not this is a significant enough fraction to be the basis of a biological signal ultimately requires further investigation. Since either slow and high amplitude or fast and low amplitude oscillation is beneficial, a possible mechanism behind radical motion could be vibration on the scale of the whole cryptochrome protein (large and slow) and on the scale of the Trp triad or FAD vibrating within the protein (small and fast). If further experiments on cryptochrome in a magnetic field confirm the existence of the peaks found here, it would add to the growing body of evidence supporting RPM, in addition to evidencing radical motion as an important part of that mechanism. With that, these results assume oscillatory movement of the radicals, which may not be the case. One goal of the optimization techniques below was to assess radical motion without an assumed radical motion function.

3.2 Optimization

The peaks seen in Fig. 9 can aid in assessment of our optimization techniques, as we expect optimization of the oscillatory motion to output values close to these peaks. The results bear out this prediction, with an amplitude of 3.49 Å and a frequency of 0.484 MHz being the optimized amplitude and frequency respectively, resulting in a yield anisotropy of 0.0982. This result was tested over several initial guess parameters, indicating that it is a global minimum. This result is consistent with the highest yield on Fig. 9, corresponding to the 4 Å amplitude at the first peak (sub-peak 1.1). Now that optimization of this model seems successful, we can move on to the more involved optimization of radical distance at every timestep. The 'blocky' look of the results is due to the thinning factor introduced, which here is 10.

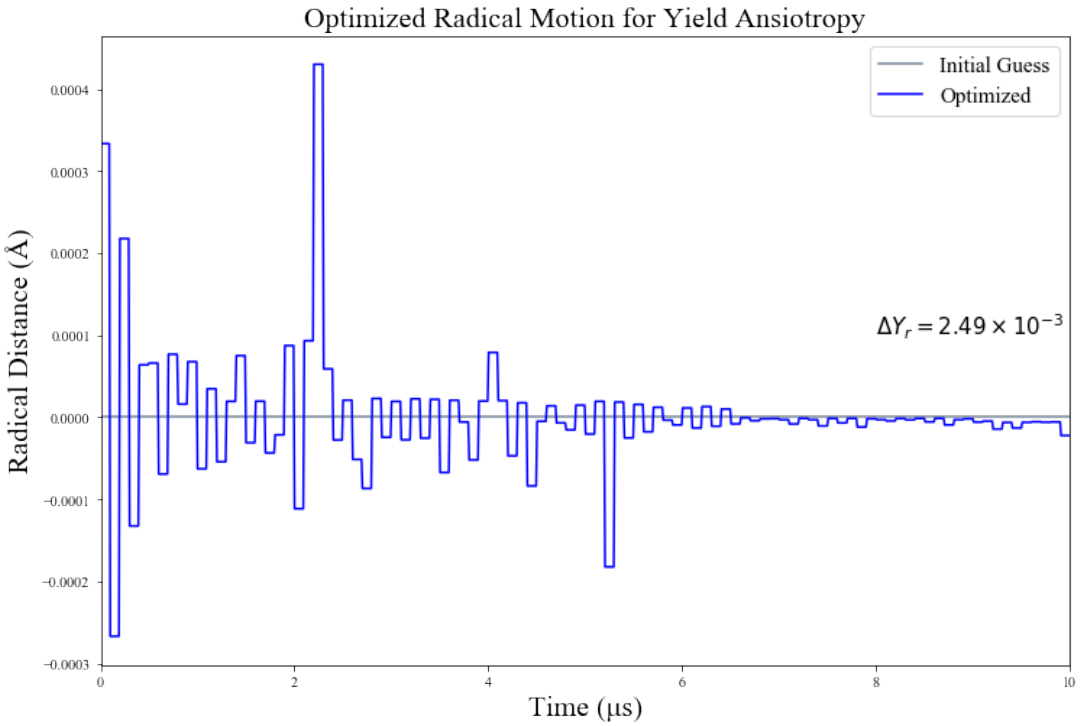

Figure 12: The optimized radical motion with initial guess motion of stationary radicals.

The results of this investigation were less successful at producing high anisotropy motion, though the results do indicate some common-sense attributes about what this motion might be like. As stated, several different initial guess parameters were tested over, which in this case did result in significantly different yield anisotropies. The best performing initial guess was the stationary radical motion, resulting in a relative improvement in anisotropy several orders of magnitude larger than others. The motion produced features a large initial jump which dwarfs subsequent motion, with semi-regular peaks throughout. The results of Fig.12 are reminiscent of oscillatory motion of two separate simultaneous frequencies, one with a large amplitude and small frequency and one with a small amplitude and large frequency. Considering the results

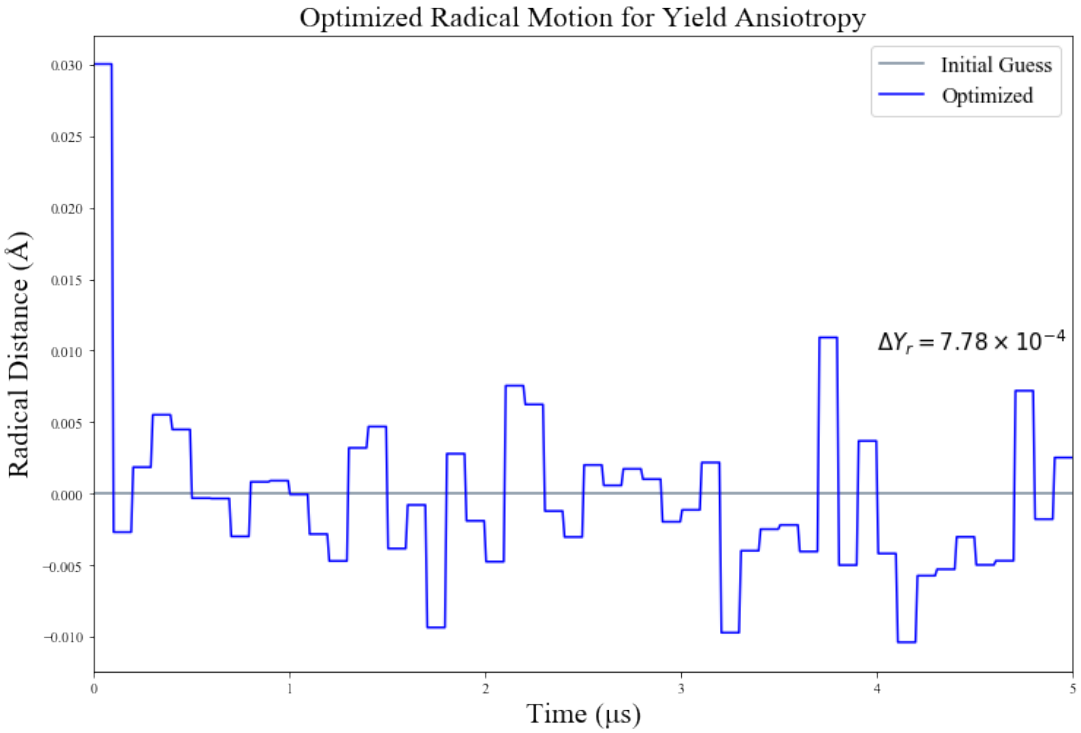

Figure 13: The optimized radical motion with initial guess motion of stationary radicals over a smaller simulated time. The relative improvement from the initial guess is indicated on each graph, $\Delta Y_R = \frac{Y_{initial} - Y_{optimized}}{Y_{initial}}$

from the previous section, it seems that this is trying to take advantage of the high anisotropy yielded at Peak 1 to large amplitudes, in addition to the high anisotropy of smaller oscillations at higher frequencies. Comparing Fig. 12 and Fig. 14 one can also see that the motion is sustained for much longer in these optimizations than other initial guesses, with the others yielding motion that dies off after the first few μs, whereas here it dies off at around 6 μs. Radical motion will no longer be optimized by the algorithm at the point where most radicals have recombined, as its impact on the final yield will be negligible. The fact that radical motion is much prolonged for the more successful optimization indicates that part of the mechanism by which it is improving the yield anisotropy is prolonging the lifetime of the radicals (i.e. reducing the recombination rate) through the radical motion.

Computational power is a strong limiting factor in these results, which can be seen by comparing Fig.12 and Fig.13, which differ only in duration of simulated time, 10 and 5 μs respectively. Halving the simulated duration resulted in a radical distance two orders of magnitude larger. This is probably due to the method by which our optimization 'explores' from the initial guess, such that with fewer timesteps more computational power could be dedicated to exploring further from the guess. This is because of a 'maxiter' parameter set when calling the minimize function which limits the number of iterations of the optimization, so as to prevent the runtime

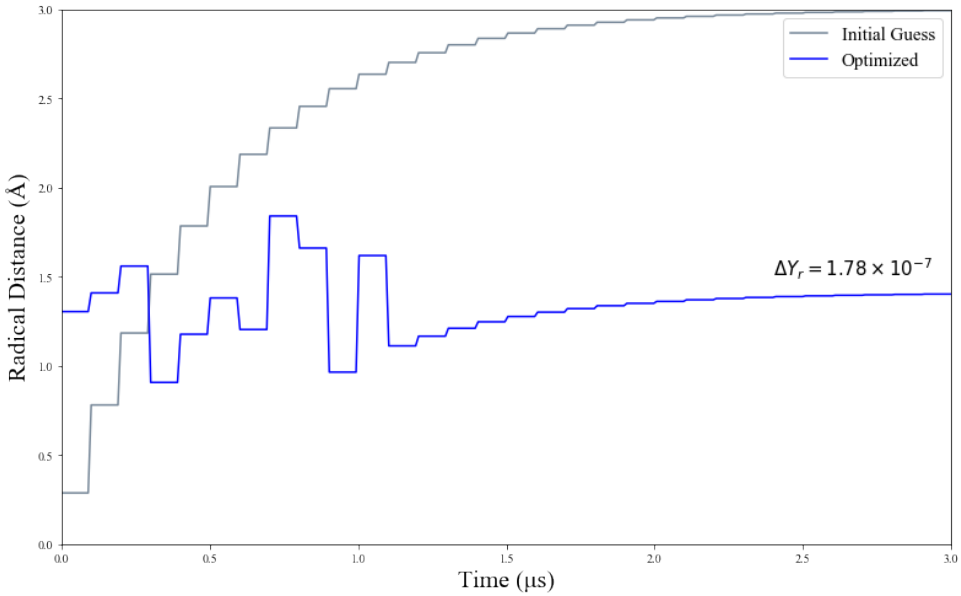

(a) Optimized radical motion from exponential approach initial guess motion.

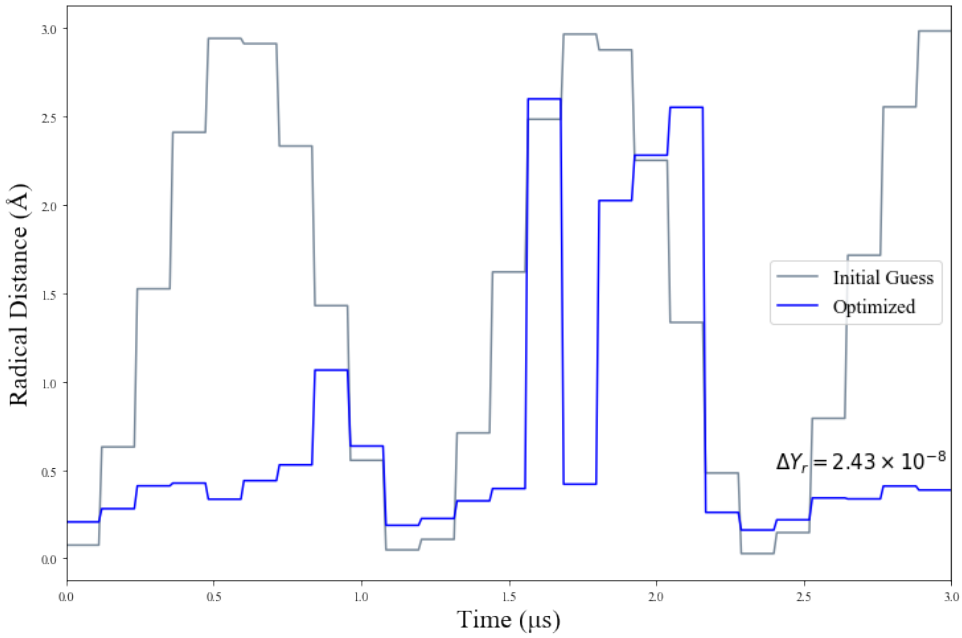

(b) Optimized radical motion from oscillatory initial guess motion.

Figure 14: Results of poorly performing initial guess functions for the optimization of radical motion.

from going over the limit. Further investigations could focus on improving the process to be less computationally expensive, or simply dedicating more processing power to it.

Other initial guess distance functions resulted in yield anisotropies four to five orders of magnitude smaller, and so will be primarily discarded as the result of local minima.

3.3 Langevin Radical Motion

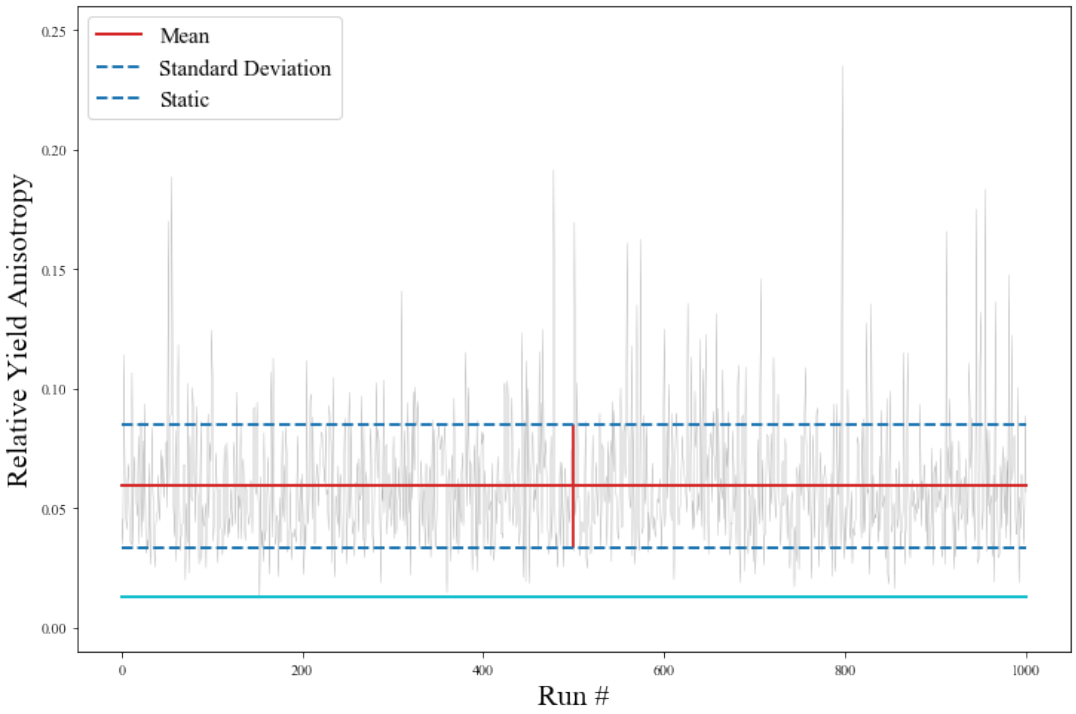

Figure 15: Improvement in yield anisotropy with random (Langevein) radical motion.

With radical motion established as a viable improvement to RPM, some consideration should also be given to what type of motion is most realistic. To this end my project partner modelled Brownian motion of the radicals, as expressed in equation 15. The yield anisotropy was different in each run due to the random nature of the distances, so an average was taken over several runs (Fig. 15). This resulted in an average relative improvement in yield anisotropy of ~0.0592, with a standard deviation of 0.02589. These improvements are comparable with those of oscillatory motion, showing that pseudo-random motion also significantly improves the sensitivity of a RPM model. This means that thermal fluctuations could, in addition to not hindering the RPM, be actively aiding it.

3.4 Dipole-Dipole Interactions

Our results so far have neglected to include dipole-dipole interactions, as they significantly increase the complexity of simulations. However, to demonstrate that these effects remain when dipole-dipole interactions are included, some data provided by our project supervisor is enclosed. In Fig.17 we see that when the radicals are stationary, the presence of exchange interactions severely inhibits the yield anisotropy. However, when oscillatory motion is included, high yield anisotropy is no longer limited to a low exchange interaction situation, meaning RPM becomes viable.

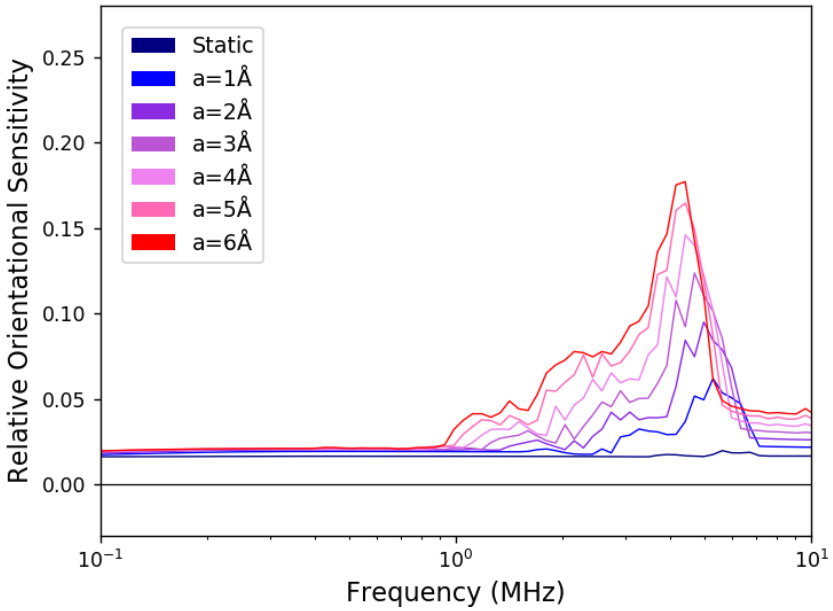

Figure 16: The effect of frequency and amplitude on yield anisotropy including dipole-dipole interactions, provided by Daniel Kattnig.

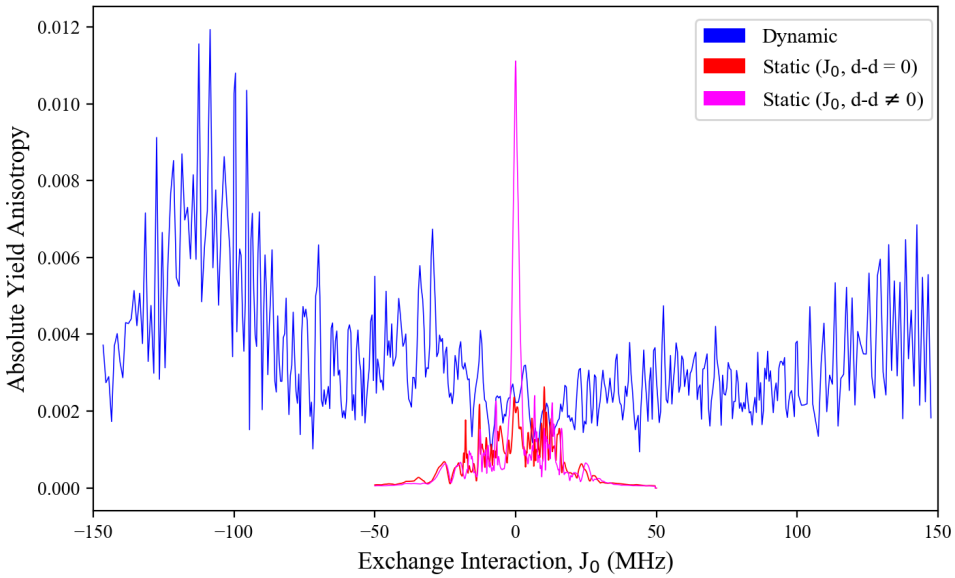

Figure 17: The increase in yield anisotropy, especially at high exchange interactions, provided by Langevin radical motion, with dipole-dipole simulations results from Daniel Kattnig. Yield anisotropy is very low at high exchange values in the static case, and fairly constant with radical motion.

Oscillatory motion also improves a dipole-dipole inclusive model with exchange interactions (Fig. 16), in a similar fashion shown above (Fig. 11), where many peaks and troughs are common to all (non-zero) amplitudes.

4 Conclusions

Overall, the addition of radical motion improves the RPM mechanism on several fronts, affording the mechanism the high sensitivity of both low recombination rates and high exchange interactions. In a no–dipole-dipole interaction model, radical motion benefited the yield anisotropy with either low frequency and high amplitude oscillation or high frequency and low amplitude oscillation. These could be physically realised in a cryptochrome protein on the scale of the whole protein, or on the scale of individual radicals oscillating relative to each other. Additionally, peaks were found in yield anisotropy that were common to all oscillation amplitudes, indicating some resonance with the system.

Optimization of oscillatory radical motion was successful, with the optimized amplitude and frequency correlating to the highest value at the highest peak in Fig. 9. This result was reproduced with a variety of initial guess values, indicating that it was not the result of the minimization function being stuck in a local minimum. However, optimization of the entire radical distance over the simulated time was more challenging, yielding limited improvement in anisotropy. Different initial guess functions did not yield the same optimized radical distances, and decreasing the simulated time significantly increased the optimized radical distances, indicating more computational power and time would have greatly benefited these attempts. The optimizations that were more successful did support the findings of two simultaneous oscillatory frequencies, as stated above, a fast and small and a slow and large oscillation. These findings also show that radical motion prolongs the lifetime of the radicals, and that the importance of radical motion dies down past around $6\,\mu s$, probably because at that point the majority of radicals have recombined.

The RPM model with dipole-dipole interactions also benefits from oscillatory radical motion, as exchange interactions limit the sensitivity of the mechanism without it. Dipole-dipole models also seem to have resonant frequencies of radical motion that are common to all amplitudes.

Finally, while much research remains to be done to obtain a complete model of a radical motion RPM model, we hope that this project has indicated interesting and fruitful avenues of investigation: the dedication of additional computation resources to finding the optimal radical motion, the investigation of resonant radical motion frequencies, the possibility of oscillatory motion on the scale of the radicals and the entire cryptochrome protein, and the in vivo sensitivity to yield anisotropies on the order of magnitude shown here.

References

[1] N. Chernetsov, D. Kishkinev, and H. Mouritsen, "A long-distance avian migrant compensates for longitudinal displacement during spring migration," *Current biology : CB*, vol. 18, pp. 188–90, 03 2008.

[2] S. Åkesson, J. Morin, R. Muheim, and U. Ottosson, "Avian orientation at steep angles of inclination: experiments with migratory white-crowned sparrows at the magnetic north pole," *Royal Society of London. Proceedings B. Biological Sciences*, vol. 268, no. 1479, pp. 1907–1913, 2001.

[3] D. Kishkinev, N. Chernetsov, A. Pakhomov, D. Heyers, and H. Mouritsen, "Eurasian reed warblers compensate for virtual magnetic displacement," *Current Biology*, vol. 25, pp. R822–R824, 10 2015.

[4] W. W. Cochran, H. Mouritsen, and M. Wikelski, "Migrating songbirds recalibrate their magnetic compass daily from twilight cues.," *Science*, vol. 304 5669, pp. 405–8, 2004.

[5] P. Hore and H. Mouritsen, "The radical-pair mechanism of magnetoreception," *Annual Review of Biophysics*, vol. 45, 06 2016.

[6] K. Schulten, C. E. Swenberg, and A. Weller, "A biomagnetic sensory mechanism based on magnetic field modulated coherent electron spin motion," *Zeitschrift für Physikalische Chemie*, vol. 111, no. 1, 1978.

[7] T. Biskup, E. Schleicher, A. Okafuji, G. Link, K. Hitomi, E. Getzoff, and S. Weber, "Direct observation of a photoinduced radical pair in a cryptochrome blue-light photoreceptor," *Angewandte Chemie (International ed. in English)*, vol. 48, pp. 404–7, 01 2009.

[8] O. Efimova and P. Hore, "Evaluation of nuclear quadrupole interactions as a source of magnetic anisotropy in the radical pair model of the avian magnetic compass," *Molecular Physics*, vol. 107, no. 7, pp. 665–671, 2009.

[9] C. Niessner, S. Denzau, J. Gross, L. Peichl, H.-J. Bischof, G. Fleissner, W. Wiltschko, and R. Wiltschko, "Avian ultraviolet/violet cones identified as probable magnetoreceptors," *PloS One*, vol. 6, p. e20091, 05 2011.

[10] T. Ritz, "Resonance effects indicate radical pair mechanism for avian magnetic compass," pp. 21005–, 03 2005.

[11] K. Kavokin, N. Chernetsov, A. Pakhomov, J. Bojarinova, D. Kobylkov, and B. Namozov, "Magnetic orientation of garden warblers (¡i¿sylvia borin¡/i¿) under 1.4 mhz radiofrequency magnetic field," *Journal of The Royal Society Interface*, vol. 11, no. 97, p. 20140451, 2014.

[12] M. K. Bowman, D. E. Budil, G. L. Closs, A. G. Kostka, C. A. Wraight, and J. R. Norris, "Magnetic resonance spectroscopy of the primary state, pf, of bacterial photosynthesis," *Proceedings of the National Academy of Sciences*, vol. 78, no. 6, pp. 3305–3307, 1981.

[13] S. Engels, N.-L. Schneider, N. Lefeldt, C. Hein, M. Zapka, A. Michalik, D. Elbers, A. Kittel, P. Hore, and H. Mouritsen, "Anthropogenic electromagnetic noise disrupts magnetic compass orientation in a migratory bird," *Nature*, vol. 509, 05 2014.

[14] O. Efimova and P. Hore, "Role of exchange and dipolar interactions in the radical pair model of the avian magnetic compass," *Biophysical journal*, vol. 94, pp. 1565–74, 03 2008.

[15] C. Timmel, U. Till, B. Brocklehurst, K. Mclauchlan, and P. Hore, "Effects of weak magnetic fields on free radical recombination reactions," *Molecular Physics*, vol. 95, no. 1, pp. 71–89, 1998.

[16] D. R. Kattnig, J. K. Sowa, I. A. Solovyov, and P. J. Hore, "Electron spin relaxation can enhance the performance of a cryptochrome-based magnetic compass sensor," *New Journal of Physics*, vol. 18, p. 063007, jun 2016.

[17] H. C. Andersen and D. Chandler, "Robert w. zwanzig: Formulated nonequilibrium statistical mechanics," *Proceedings of the National Academy of Sciences*, vol. 111, pp. 3–10, Jul 2014.

[18] F. Cailliez, P. Müller, T. D. R. Firmino, P. Pernot, and A. de la Lande, "Energetics of photoinduced charge migration within the tryptophan tetrad of an animal (6-4) photolyase.," *Journal of the American Chemical Society*, vol. 138 6, pp. 1904–15, 2016.